RESEARCH ARTICLE | JULY 07 2023

System dynamics monitoring using PIC micro-controller-based PLSE 🕞

Special Collection: Ordinal Methods: Concepts, Applications, New Developments and Challenges

Guy Morgand Djeufa Dagoumguei 🆔 ; Samuel Tagne 🆔 ; J. S. Armand Eyebe Fouda ✉ 🆔 ; Wolfram Koepf

⊕ Check for updates

🌐
View Online

↗
Export Citation

Articles You May Be Interested In

Development and testing of a low-cost portable soil apparent electrical conductivity sensor

AIP Advances (March 2025)

Uncertainty of financial time series based on discrete fractional cumulative residual entropy

Chaos (October 2019)

Experimental investigation of the chaotification of a Duffing-like electronic oscillator under two-frequency excitation

Chaos (June 2024)

System dynamics monitoring using PIC micro-controller-based PLSE Ⓕ

View Online   Export Citation   CrossMark

Guy Morgand Djeufa Dagoumguei,[1,a)] Ⓘ Samuel Tagne,[1,b)] Ⓘ J. S. Armand Eyebe Fouda,[1,c)] Ⓘ
and Wolfram Koepf[2,d)]

AFFILIATIONS

[1] Department of Physics, University of Yaoundé I, Faculty of Science, P.O. Box 812, Yaoundé, Cameroon
[2] Institute of Mathematics, University of Kassel, Heinrich-Plett-Str. 40, 34132 Kassel, Germany

Note: This paper is part of the Focus Issue on Ordinal Methods: Concepts, Applications, New Developments and Challenges.
[a)] **Electronic mail:** mdjeufa@yahoo.com
[b)] **Electronic mail:** samueltagne90@yahoo.com
[c)] **Also at:** Institute of Mathematics, University of Kassel, Heinrich-Plett-Str. 40, 34132 Kassel, Germany. **Author to whom correspondence should be addressed:** efoudajsa@yahoo.fr. **URL:** http://www.mathematik.uni-kassel.de/~fouda/
[d)] **Electronic mail:** koepf@mathematik.uni-kassel.de. **URL:** http://www.mathematik.uni-kassel.de/~koepf/

ABSTRACT

The permutation largest slope entropy (PLSE) algorithm has been shown to be effective to distinguish between regular and non-regular dynamics from time series analysis. However, as it is the case for many non-linear time series analysis algorithms, such a characterization is locally made and does not allow one to capture some micro-phenomena, such as intermittency, that may occur in the system behavior. This paper presents a PIC micro-controller based implementation of the PLSE for a real-time monitoring of system dynamics. The PLSE algorithm is optimized to fit the program and data memory of low-end processors using the XC8 compiler and the MPLAB X IDE. The resulting algorithm is implemented on the PIC16F18446 and deployed on the Explorer 8 development board. The effectiveness of the developed tool is validated by considering an electrical circuit of the Duffing oscillator that can generate both periodic and chaotic dynamics. By comparing the PLSE values with the phase portraits and previous results on the Duffing oscillator circuit, the developed tool efficiently allows one to monitor the behavior of dynamical systems.

The permutation largest slope entropy (PLSE) is implemented on a PIC16F18446 micro-controller for online data analysis. An example of applications on the Duffing electrical circuit is successfully presented, from where the efficiency of ordinal methods for a real-time monitoring of real-life dynamical systems can be concluded. These results constitute a new step in the research for systematic applications of ordinal methods as the user is freed from complex calculations due to the search for optimal parameter setting, thereby simplifying the use of the method for nonspecialists.

I. INTRODUCTION

During the last two decades, quantitative methods, including ordinal pattern-based methods, are increasingly used to characterize system behavior from time series. Prior to the seminal paper of Bandt and Pompe on permutation entropy,[1] an attempt for quantifying the complexity of a system from time series was proposed by the Rosenstein algorithm for computing the maximal Lyapunov exponent (MLE).[2] However, this algorithm is noise sensitive and time costly and requires the phase space reconstruction. Another popular algorithm developed approximately at the same time as the Bandt–Pompe algorithm is the 0–1 test by Gottwald and Melbourne.[3,4] This method defines the asymptotic growth rate K to detect regular dynamics with $K = 0$ value and non-regular dynamics with $K = 1$. In practice, the 0–1 test is sensitive to the sampling frequency and is also time costly. Theoretical approaches, such as the Lyapunov exponent,[5,6] Kolmogorov–Sinai (KS) entropy,[7] correlation dimension,[8] and many others are difficult to estimate from a finite data set.

Subsequently, ordinal pattern-based methods have been introduced in 2002 by Bandt and Pompe.[1] They defined the permutation entropy (PE) demonstrated to be effective for the

analysis of time series. Likewise, it is robust against noise, easy to implement, and runs faster than the previous other methods. Ordinal methods are being applied in fields, such as physics, finance, economics, biology, and meteorology.[9] However, the PE does not necessarily take zero values for regular dynamics, which makes their detection difficult. By considering such a limitation of the PE, various ordinal pattern-based algorithms have been developed. Among them, one can quote the conditional entropy of ordinal patterns (CEOP) developed by Unakafov and Keller to estimate the complexity of dynamical systems.[10,11] The CEOP is closer to zero for regular dynamics than the PE, thus improving their detection.

In order to further improve the detection of regular dynamics with zero entropy, Eyebe *et al.* developed the permutation largest slope entropy (PLSE).[12,13,25] The main idea in this approach is to characterize any limit-cycle by its phase space period defined to be the largest slope.[12] Similar to other ordinal pattern-based methods, the PLSE applies to time series and does not require any prior knowledge on modeling equations of the system. A comparative study, including the PLSE, the 0–1 test, and the MLE, has demonstrated the effectiveness of the PLSE for the analysis of real-world data.[13] Such a comparison was made with data locally collected on time and does not allow one to conclude on the long-term dynamics of the system. Indeed, the analysis of local data is valid only for the underlying observation and does not describe the whole dynamics of the system. For instance, a system exhibiting intermittent behavior may be detected as stable while collecting the data during a stable time slot. An example of such a system is the cardiovascular system in the case of arrhythmia. Therefore, a real-time monitoring of the system is required. Real-time monitoring tools allow one to understand and control several phenomena of daily life. Some examples of real-time monitoring concern heartbeats, weather data, eye jumps, rainfall measurements, industry forecasts, interest rates, and the brain system.[14]

Taking into account the ability of the PLSE to analyze real-world data and its speed performance, this paper aims at developing a PLSE-based real-time monitoring system. The system is developed using the PIC16F18446. For the PLSE algorithm to run on the above low-end processor, an optimized algorithm is developed using the XC8 compiler and MPLAB X IDE as the development platform. The performance of the resulting system, deployed on the Explorer 8 board, is assessed using the Duffing oscillator electrical circuit. Although the idea of developing PIC-based systems is not new,[15–17] it is the first attempt to the best of our knowledge for developing a real-time monitoring tool for the entropy measure based on ordinal patterns. The idea is to simplify and facilitate the inclusion of ordinal pattern-based algorithms to nonlinear data analysis.

This paper is organized as follows: Sec. II presents the PIC micro-controller (PMC)-based implementation of the PLSE, Sec. III is devoted to the analysis and discussion of the experimental results, while Sec. IV ends the paper with a conclusion.

II. PIC MICRO-CONTROLLER IMPLEMENTATION OF THE PLSE

A. Brief presentation of the PLSE algorithm

The PLSE was inspired by the PE. However, instead of considering permutations as ordinal patterns, the PLSE uses the largest slope obtained by differentiating the corresponding permutation. Let $\{x_t\}_{t=0,1,\ldots,T-1}$ be a time series of length T and $\mathbf{x}_t = (x_t, x_{t+\tau}, \ldots, x_{t+(n-1)\tau})$ an embedding vector of length n. n is known as the embedding dimension, and $\tau \in \mathbb{N}_{\geq 1}$ is the delay time of samples. A permutation π_t of order $n-1$ is obtained by sorting neighboring values in $\mathbf{x}_t$ into an ascending order and considering the resulting time index sequence. Identical values are sorted by an ascending order of their time index. The largest slope $S_t = \max(\{s_i\})$ of the above permutation π_t is then defined as the maximal value of the set of consecutive differences of time indices $s_i = \pi_t(i + 1) - \pi_t(i), 0 \leq i \leq n - 1$.[12] For a given embedding dimension n, there are n distinct largest slopes, namely, $\mathscr{S} = \{-1, 1, 2, \ldots, n-1\}$. In addition to the delay time of samples τ, the delay time of embedding vectors $1 \leq t_0 \leq n - 1$ was also defined as the delay between consecutive embedding vectors. The PLSE is, therefore, defined as

$$h(n) = -\sum p(S) \log(S) / \log(n), \tag{1}$$

where

$$p(S) = \frac{\#\{t \mid 0 \leq t \leq T - (n-1)\tau - 1, S_t = S\}}{T - (n-1)\tau} \tag{2}$$

is the probability of obtaining $S_t = S$. It was shown in Ref. 12 that L-periodic dynamics are characterized by a single largest slope $S = L$ if $n > L$. In such a case, regular dynamics are characterized by $h = 0$, whereas $h > 0$ for non-regular dynamics. The PLSE has also been shown to be fast and robust against noise. However, we should emphasize that the detection results strongly depend on the embedding dimension n. Indeed, the largest period that can be detected by the PLSE for $\tau = 1$ is $L = n - 1$. More details on the definition of the PLSE method can be found in Ref. 12. The MATLAB code of the PLSE is available at https://www.mathematik.uni-kassel.de/~fouda/.

B. The differential dynamical quantization (DDQ)

For the PLSE to be efficiently applied to real-world data, the DDQ is required. Indeed, real-world data are always noise contaminated from various sources of perturbation. For analog data, two main types of noise are distinguished: the observational (additive) noise and the dynamical (internal to the system) noise. For digital data, in addition to the previous two types, the quantization and sampling noise should be considered. The DDQ is a nonlinear approach, which consists of affecting a single value (quantization) to those data, which are approximately the same in the data series. It then allows one to reduce the amount of noise in the acquired data by applying a noise threshold that depends on the embedding vector[13,18] and is preferred to common noise reduction techniques as it is fast and easy to implement.

Thus, given a sequence $\{x_t\}$ and a threshold or noise tolerance η (quantization step), values in $\{x_t\}$ are first sorted into an ascending order to obtain a sequence $\{u_j\}$ in which all equal values are neighbors. Thereafter, u_j and u_{j+1} are compared and set to $u_{j'+1}$ if $|u_j - u_{j+1}| < \eta$ and $j' < j$; otherwise, these values are left unchanged. j' is such that $|u_{j'} - u_{j'+1}| \geq \eta$. At the end of the quantization process, the values in $\{u_j\}$ are reordered as in $\{x_t\}$ to obtain the quantized sequence $\{v_t\}$. η is set as a percentage of the maximal value of the underlying sequence.
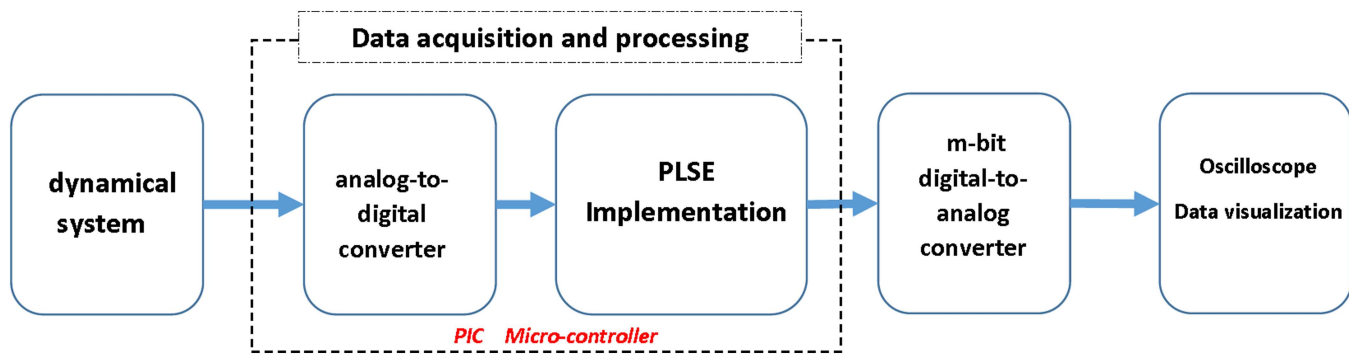
FIG. 1. Synoptic of the PLSE implementation based on the PMC.

C. Description of the PMC-based PLSE algorithm

The synoptic of the PMC-based system to be realized is shown in Fig. 1. Implementing the PLSE on low-end processors, such as PMC, is a challenging task as there is not enough memory space for both program instructions and data variables. While considering an embedding length n, the implementation of the PLSE requires the storage of an n-length histogram $\mathbf{H}$ and an n-length embedding vector $\mathbf{x}$ containing the data sequence to be analyzed. The type of the above variables depends, respectively, on the observation length and the precision of the data to be analyzed. For an observation length $T < 256$, for example, $\mathbf{H}$ can be set as an n-length vector of 1-byte encoded values. Another important variable is the n-length embedding vector π. In order to efficiently manage the small storage space available in PMC, a single embedding vector $\mathbf{x}$ is saved and updated each time a new sample is acquired. Similarly, a single vector π is saved and updated with $\mathbf{x}$. By this approach, a largest slope S is computed at each update of $\mathbf{x}$ and $\mathbf{H}(S)$ is incremented. $\mathbf{H}(\mathbf{0})$ is incremented in the case $S = -1$. For a given observation length T, the probability of each largest slope that has occurred is obtained as

$$p(S) = \frac{\mathbf{H}(S)}{T}, \tag{3}$$

and the entropy is easily deduced from Eq. (1). Figure 2 gives the flow chart of the PMC algorithm of the PLSE. The value of the PLSE is updated each N acquired samples, and the histogram is reset after analysis of T samples. For an m-bit precision output of the PMC, the entropy is obtained as

$$h(n) = \frac{\sum_{i=0}^{m-1} 2^i \cdot b_i}{2^m}. \tag{4}$$

In case a digital-to-analog converter (DAC) is used, the entropy is obtained by dividing the DAC output voltage by 5 V, as the PMC output is ranged between 0 and 5 V.

D. Implementation of the PMC-based PLSE on PIC16F18446

The PIC16F18446 is an 8-bit micro-controller, including core independent peripheral (CIP) devices, and a 12-bit resolution analog-to-digital converter (ADC). It presents up to 28 KB program Flash memory and 2 KB data SRAM memory that is useful for the implementation of the above PLSE algorithm, although large embedding dimension values cannot be set. The largest embedding is $n = 40$ for an $\mathbf{H}$ set as a vector of 2-byte encoded numbers. Such an embedding dimension is enough for the detection of regular dynamics with weak periods as it is the case for many common dynamical systems. As shown in Ref. 12, dynamics with large periods can be detected by considering $\tau > 1$ or by analyzing the series of local maxima of the underlying time series.

We implemented the algorithm in Fig. 2 by setting $N = 128$, $T = 32\,768$, and $n \leq 20$ and compiled it with XC8 in the MPLAB X IDE environment. The data memory usage is 15%, while the program memory usage is 30%. We set the clock frequency as $F_{osc} = 32$ MHz, and the pre-scaler value for the ADC is set as $r = 32$, which fixed its sampling frequency as $F_s = 71.4$ kHz. The computed value of the PLSE is sent out to PORTC and then converted using an external DAC based on an R-2R network.[19]

III. RESULTS AND DISCUSSION

In this section, we apply the implemented analysis tool to the logistic map and the Duffing oscillator. The logistic map is internally realized in the micro-controller, and its output is directly applied to the PLSE algorithm. The Duffing oscillator is implemented on a separate board, and its output connected to the micro-controller ADC. In this case, as the Duffing oscillator outputs alternatively positive and negative values, an offset is applied to its output for it to range between 0 and 5 V.

A. Analysis of the logistic map dynamics

The logistic map is described by the following equation:

$$x_{k+1} = \mu x_k (1 - x_k), \tag{5}$$

where $0 < \mu \leq 4$ is the control parameter. Phase space values are such that $0 \leq x_k < 1$, where x_0 is the initial condition of the map. We used MATLAB to compute the PLSE of the logistic map for $3.5 \leq \mu \leq 4$ and $x_0 = 0.45$. Values of x in the MATLAB environment are double precision. We set $n = 20$ and $\eta = 0$ for us to detect
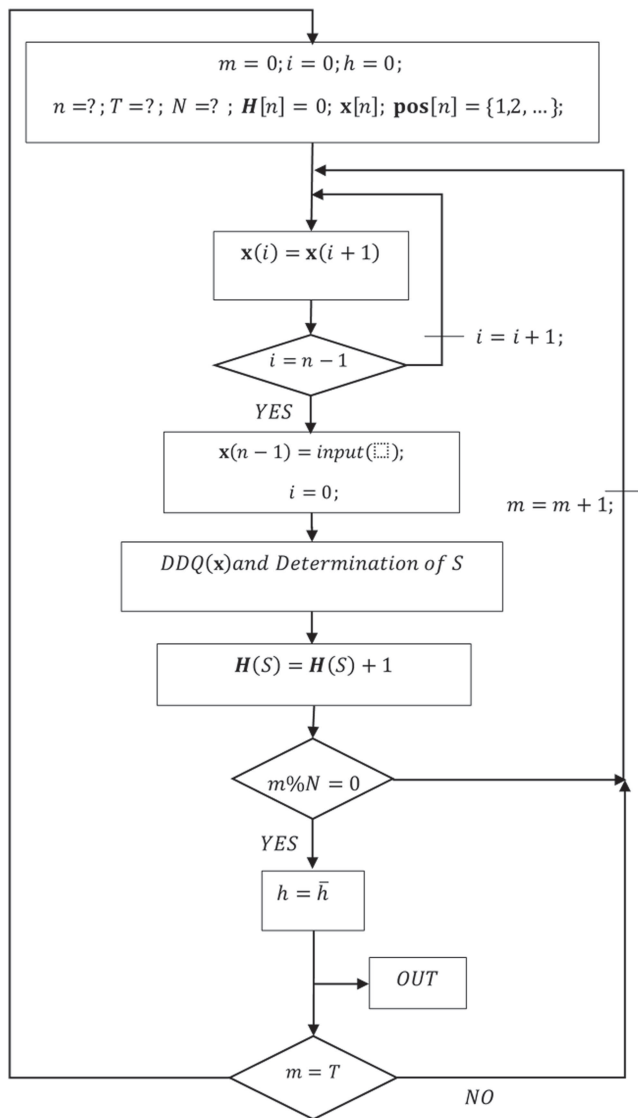
FIG. 2. Flow chart of the PMC-based PLSE algorithm.

FIG. 3. PLSE bifurcation diagram of the logistic map.

the logistic map into 12-bit encoded integers and the entropy values into 8-bit integers as described in Eq. (4). Therefore, we can conclude that the data conversion reduces the period of limit-cycles, while the randomness of the chaotic map is maintained quite unchanged. Such a reduction of the period of limit-cycles is an advantage for our PMC-based tool as it allows one to detect limit-cycles with large periods using small embedding dimensions. Thus, the results obtained confirm that the embedded PLSE algorithm matches the MATLAB code and, therefore, can be applied for the experimental system monitoring.

B. Analysis of the Duffing oscillator dynamics

1. Brief recall of the Duffing oscillator

The Duffing oscillator is one of the prototypes indicated for the study of nonlinear chaotic dynamics.[20–22] Its electrical circuit proposed in Refs. 23 and 24 is shown in Fig. 4(a). It

all the limit-cycles whose periods are less than 20. The corresponding bifurcation diagram is shown in Fig. 3. According to this figure, $\mu = 3.5$, $\mu = 3.53$, and $\mu = 3.565$ correspond to period-4, period-8, and period-16 limit-cycles, respectively, and the system exhibits chaotic dynamics for $\mu = 3.65$ and $\mu = 4$.

In order to estimate the impact of data conversion on the underlying dynamics, we converted double precision values into 12-bit encoded integers in the PIC code. We ran the PMC-based tool for $n = 5, 12, 20$, $\mu \in \{3.5, 3.53, 3.565, 3.65, 4\}$ with $\eta = 0$ and compared the results obtained with those of the MATLAB simulation. The corresponding entropy values are summarized in Table I. The difference observed comes from the rounding error while converting
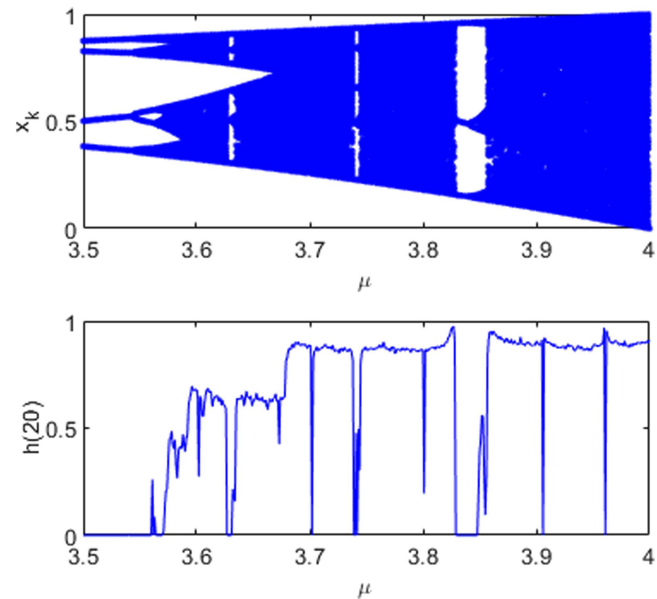
TABLE I. Comparison of MATLAB and PIC-based PLSE algorithms.

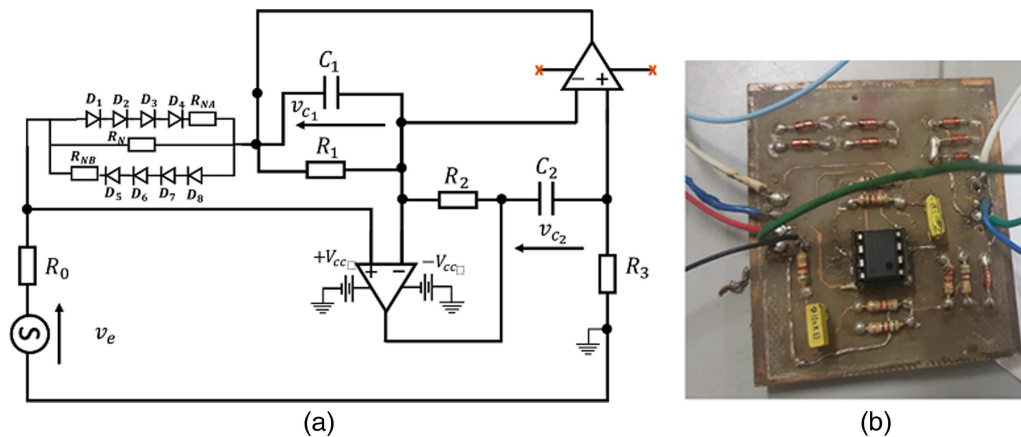|	MATLAB			PIC		
	n			n		
μ	5	12	20	5	12	20
3.5	0	0	0	0	0	0
3.53	0.6460	0	0	0	0	0
3.565	0.6460	0	0	0.6470	0	0
3.65	0.6566	0.5376	0.5561	0.6549	0.5450	0.5803
4	0.8516	0.8279	0.7956	0.8470	0.8274	0.8000

FIG. 4. Duffing oscillator: (a) electrical model and (b) electrical circuit.

has been implemented as shown in Fig. 4(b) and analyzed in Ref. 13. The resistor values are chosen as $R_1 = 5.1\,k\Omega$, $R_2 = 1\,k\Omega$, $R_3 = 1\,k\Omega$, and $R_4 = 3.2\,k\Omega$ and capacitor values as $C_1 = 10$ nF and $C_2 = 2.2$ nF. It is characterized by a cubic nonlinear element of the form $i(x) = ax + bx^3$ where a and b are constants. Let us denote the voltage across the capacitors C_1 and C_2 by v_{C_1} and v_{C_2}, respectively. The Duffing state equations are given as

$$\begin{cases} \dfrac{dv_{C_1}}{dt} = -\dfrac{1}{R_1 C_1} v_{C_1} - \dfrac{1}{R_2 C_1} v_{C_2}, \\[2mm] \dfrac{dv_{C_2}}{dt} = \dfrac{R_0}{R_3 C_2}\left(av_{C_1} + bv_{C_1}^3\right) + \dfrac{1}{R_3 C_2} v_e(t), \end{cases} \quad (6)$$

where $v_e(t)$ is a sinusoidal forcing voltage of the form $v_e(t) = v_m \sin(2\pi f t)$ with frequency f and amplitude v_m.

2. Experiment setup and data acquisition

For the developed PMC-based tool to apply to any experimental system, a data preconditioning is required. Indeed, the PMC is power supplied with 5 V DC and can process only input data in the range of 0–5 V. The preconditioning module is placed prior to the ADC of the PMC and applies an offset voltage $V_{off} = 2.43$ V to the output of the Duffing oscillator, while controlling its amplitude to vary between 0 and 5V. The controlled analog voltage is then applied to the 12-bit ADC of the PIC16F18446 at sampling rate $F_s = 71.4$ kHz. The Duffing circuit is forced with a sine wave with frequency $f = 6.67$ kHz and amplitude $0 \le v_m \le 6V_{rms}$. All the forcing amplitudes in the paper are taken as root mean squared (rms) values. The micro-controller is programmed through the Explorer 8 development board using the PICkit3 programmer. The complete experiment is shown in Fig. 5.

3. Analysis of experimental data

The PLSE was directly applied to the entire continuous time series acquired from the Duffing oscillator. For a classical analysis, an observation time T is set during which a data series is recorded, and thereafter, embedding vectors of size n taken at step size τ are constructed. In our approach, a single n-length embedding vector $\mathbf{x}_t$ initially set at $\mathbf{x}_0 = 0$ is considered and updated for each sampling time; for example, for $n = 3$ and $\tau = t_0 = 1$, the embedding vector
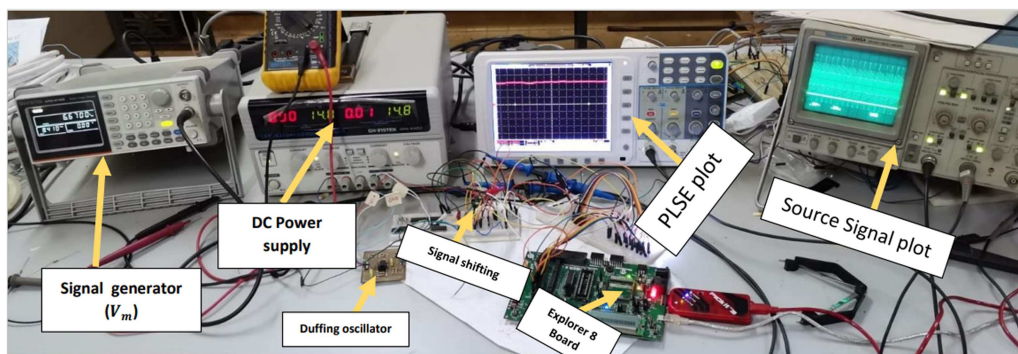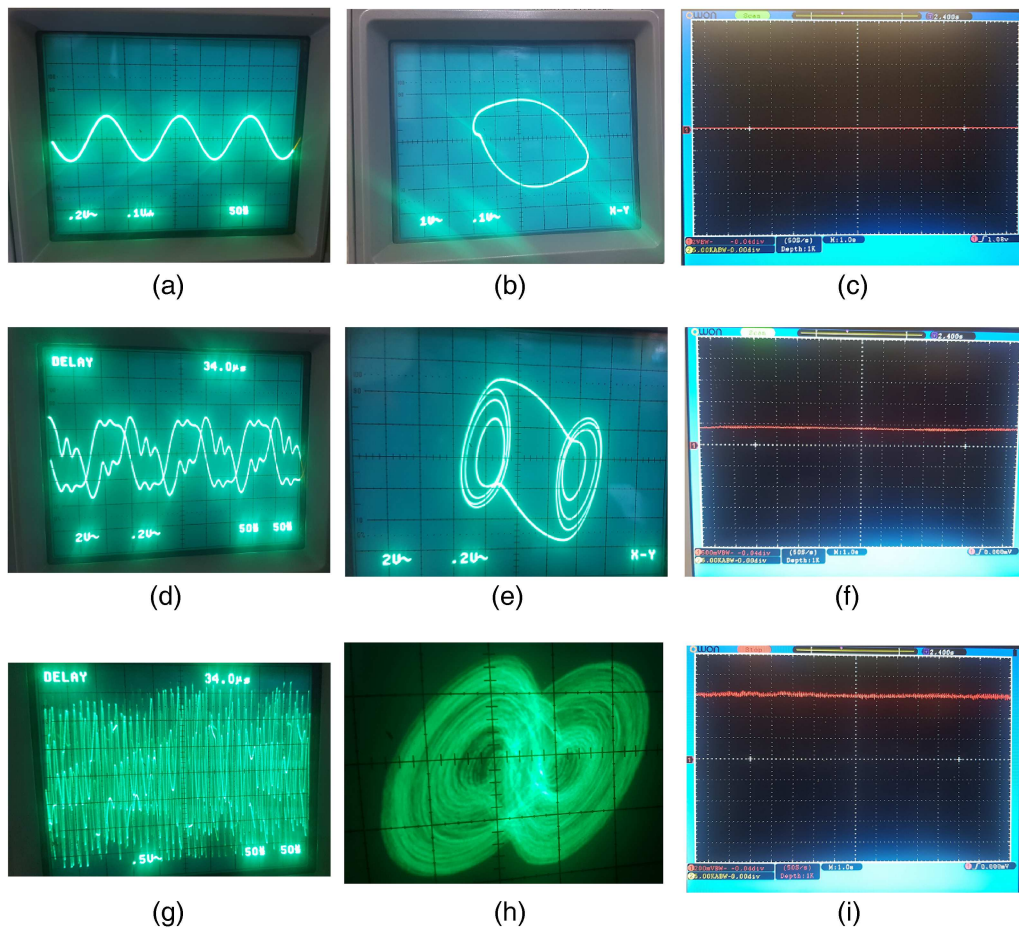

FIG. 5. Experimental setup.

FIG. 6. Example of experimental results: time series [(a), (d), and (g)], phase portraits [(b), (e), and (h)], and corresponding PLSE [(c), (f), and (i)].

$\mathbf{x}_t$ evolves as follows: $x_0 = \{0, 0, 0\}$, $\mathbf{x}_1 = \{0, 0, x_1\}$, $\mathbf{x}_2 = \{0, x_1, x_2\}$, $\mathbf{x}_3 = \{x_1, x_2, x_3\}$, $\mathbf{x}_4 = \{x_2, x_3, x_4\}$ .... A single permutation π_t is also set and updated at each sampling step. By this approach, the data memory is saved, and relatively large embedding dimensions can be considered. For the data analysis with our tool, we set $\tau = t_0 = 1$ and $n = \{5, 12, 20\}$. The histogram $\mathbf{H}_t$ is updated at each sampling step and re-initialized at each $T = 32\,768$ sampling steps, while the PLSE is computed and displayed at each $N = 128$ sampling steps. Figure 6 shows some examples of entropy measure for $n = 20$, $\eta = 3.66\%$, and the corresponding dynamics. From the left to the right are shown the time series, the phase portrait, and the PLSE plot. The first line shows an example of limit-cycle obtained with $v_m = 0.545\,\mathrm{V_{rms}}$, $\eta = 3.66\%$, and the corresponding entropy $h(20) = 0$. The dynamics on the second line is obtained for $v_m = 1.7\,\mathrm{V_{rms}}$, $\eta = 3.66\%$; its entropy is $h(20) = 0.09$ and corresponds to weakly chaotic behavior. In the third line, the chaotic dynamics is obtained with a forcing voltage of $v_m = 2.45\,\mathrm{V_{rms}}$, $\eta = 3.66\%$, and the corresponding PLSE value is $h(20) = 0.20$. While comparing phase portraits of the above dynamics with the

corresponding entropy values, it appears that our tool successfully applies to the characterization of real-world data. The PLSE increases with the complexity of the dynamics under investigation.

We then applied the PLSE to experimental data obtained by varying the amplitude v_m of the forcing voltage and the noise tolerance η and plotted the corresponding experimental bifurcation diagrams of the Duffing system. The results are summarized in Fig. 7. Figure 7 shows the dependence of the entropy value on the embedding dimension and the noise tolerance. We can observe that the noise tolerance mostly affects limit-cycles as their entropy significantly decreases as η increases. The increase of both n and η allows one to reduce the entropy of limit-cycles with a large period. Indeed, the superposition of the noise effect on regular dynamics with large periods significantly changes their behavior, thus looking as non-regular. The PLSE algorithm is sensitive to η as the embedding dimension increases.

Figure 8 shows that the characterization of the system for non-regular dynamics does not change with the parameter setting. The bifurcation diagrams obtained for $n = 12$, $\eta = 4.88\%$ and $n = 20$,
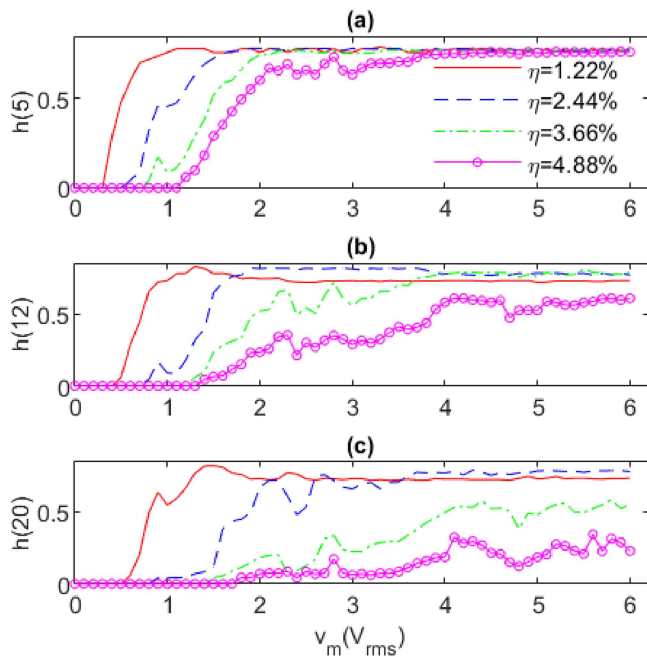
FIG. 7. Experimental bifurcation diagram of the PLSE with respect to the forcing voltage v_m for various embedding dimensions and noise tolerances: (a) $n = 5$, (b) $n = 12$, and (c) $n = 20$.

FIG. 8. Experimental bifurcation diagram of the PLSE with respect to the forcing voltage v_m.

$\eta = 3.66\%$ behave quite similar. However, the DDQ is required for periodic dynamics to be detected. By setting $\eta = 0\%$, all the dynamics are detected as non-regular due to the presence of noise in the acquired data. Thus, like in the case of the logistic map, the DDQ acts as a converter that reduces the precision of the input data sequence. Table II summarizes some examples of entropy values for comparison between $n = 12$, $\eta = 4.88\%$ and $n = 20$, $\eta = 3.66\%$ results.

Figure 8 also clearly indicates that the system exhibits periodic dynamics for $0 \le v_m \le 1.6\,V_{rms}$ as $h(5) = 0$. Such a periodic detection is confirmed by the phase portraits in Fig. 9 where limit-cycles are evidently observed for $v_m = 0.3\,V_{rms}$, $v_m = 0.8\,V_{rms}$, and $v_m = 1.6\,V_{rms}$. For $v_m \ge 1.7\,V_{rms}$, the PLSE is greater than 0. Such a result may indicate chaotic dynamics or limit-cycles with large periods. Although the phase portraits for $v_m = 1.6\,V_{rms}$ and $v_m = 1.7\,V_{rms}$ look similar, the PLSE clearly indicates a difference between the two states of the system. Between $v_m = 1.7\,V_{rms}$ and $v_m = 2.2 V_{rms}$, a uniform increase of $h(20)$ from 0 to 0.202 is observed, but the corresponding phase portraits seem periodic. The increase of the PLSE may be interpreted as an increase of
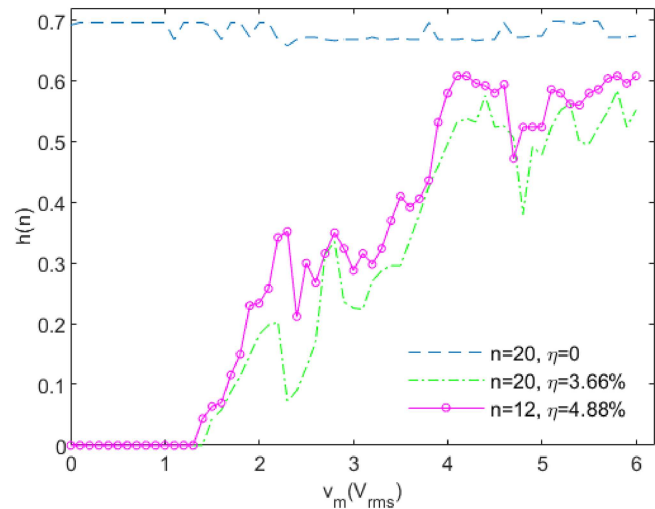
the period of the corresponding limit-cycles, thus symbolizing the transition of the system from periodic to chaotic dynamics. From $v_m = 2.3\,V_{rms}$ to $v_m = 2.6\,V_{rms}$, the phase portraits indicate chaotic behaviors. The corresponding PLSE values increase from $h(20) = 0.07$ to 0.17. It should be emphasized that phase portraits in this forcing region are different when increasing or decreasing the forcing voltage, but the entropy range does not change. Phase portraits corresponding to the increase of v_m look like limit-cycles, whereas those corresponding to the decrease of v_m indicate chaotic motions (see Fig. 9). From $v_m = 2.7\,V_{rms}$ to $v_m = 3.6\,V_{rms}$, the PLSE fluctuates between 0.31 and 0.34. Such a slight increase of the PLSE is also confirmed by the phase portraits whose density slightly increases. From $v_m = 3.7\,V_{rms}$ to $v_m = 4.4\,V_{rms}$, the entropy increases from 0.38 to 0.58. Between $v_m = 4.4\,V_{rms}$ and $v_m = 6\,V_{rms}$, the entropy fluctuates between 0.55 and 0.58. In this region, phase portraits indicate a mixture of limit-cycles with large periods and weakly chaotic dynamics.

By comparing the PMC-based PLSE results with our previous work, we observe a consistency between the results in Refs. 12 and 13 and those presented in this paper for $v_m \le 1.6\,V_{rms}$. The use of the DDQ with different noise tolerances allows one to appreciate the complexity of the underlying dynamics and to compensate the smallness of the value of n admissible in the PMC-based algorithm. Although the PLSE is not a complexity measure, it nevertheless exhibits some differences between dynamics, as confirmed in this paper. The robustness against noise introduced by the DDQ makes

TABLE II. Example of forcing voltages v_m and corresponding normalized PLSE values $h(n)$ for $n = 12$, $\eta = 4.88\%$ and $n = 20$, $\eta = 3.66\%$, respectively.

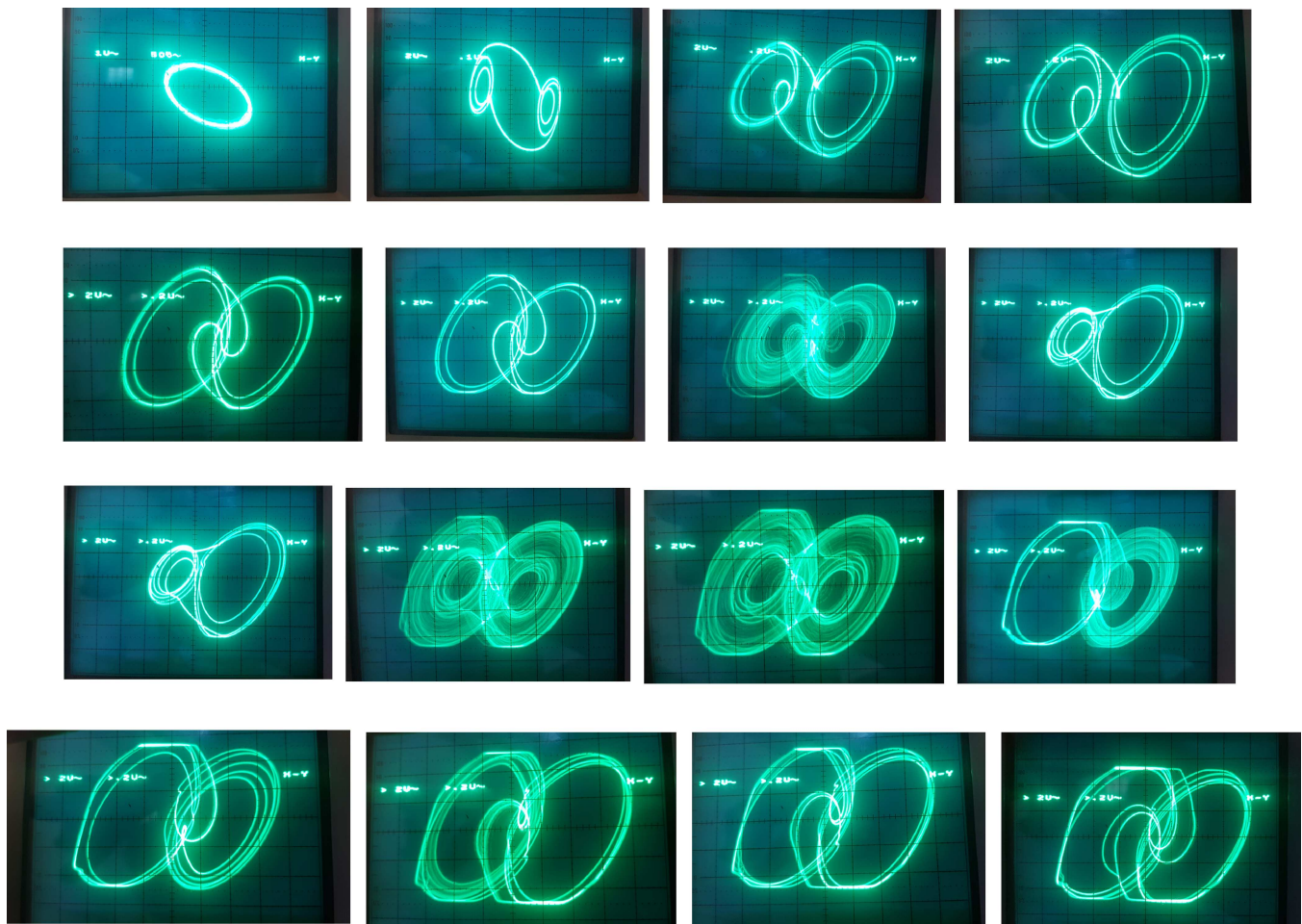| v_m (V_{rms})	0.3	0.8	1.7	1.8	2.2	2.7	2.8	3.1	3.2	3.9	4.2	4.7	5.0	5.3	6
$h(12)$	0	0	0.12	0.15	0.34	0.32	0.34	0.32	0.30	0.53	0.61	0.47	0.52	0.56	0.61
$h(20)$	0	0	0.09	0.11	0.20	0.31	0.35	0.22	0.27	0.46	0.54	0.51	0.48	0.56	0.55

FIG. 9. Experimental phase portraits.

the proposed tool for real-life dynamical system monitoring useful, hence for a rapid characterization of system dynamics. The results, thus, obtained in this paper confirm the effectiveness of the PLSE, hence ordinal pattern-based algorithm for real-time analysis of real-world data. Developing an online data analysis tool makes the inclusion of ordinal pattern methods in future nonlinear time series analysis applications easier. Given the limited memory space of the PIC16F18446, the maximal embedding dimension that could be set is $n = 24$, which makes difficult the detection of periodic dynamics with period greater than $L = 24$.

IV. CONCLUSION

Twenty years after the introduction of ordinal pattern-based data analysis by Bandt and Pompe, there is still a need for a systematic application of ordinal methods. This paper has presented a PMC-based implementation of the PLSE for facilitating the inclusion of ordinal methods in experimental data analysis. Such an

approach is to confirm theoretical statements about the speed performance, robustness against noise, and ease of implementation of ordinal methods. We used a low-end processor, namely, the PIC16F18446, with basic programming using the XC8 compiler to achieve a real-time implementation of the PLSE. The experimental analysis results obtained with the Duffing oscillator circuit attest the efficiency of the PMC-based PLSE for the detection of regular dynamics, as well as the characterization of non-regular dynamics. The PMC-based implementation thus realized opens new perspectives for the use of ordinal methods for the resolution of real-life problems in various research fields, especially in physics and biology where monitoring system dynamics can be crucial.

DEDICATION

This paper is dedicated to the memory of Professor Karsten Keller.

AUTHOR DECLARATIONS

Conflict of Interest

The authors have no conflicts to disclose.

Author Contributions

Guy Morgand Djeufa Dagoumguei: Data curation (equal); Formal analysis (equal); Methodology (equal); Validation (equal); Visualization (equal); Writing – review & editing (equal). **Samuel Tagne:** Conceptualization (equal); Data curation (equal); Formal analysis (equal); Investigation (equal); Methodology (equal); Validation (equal); Visualization (equal); Writing – original draft (equal); Writing – review & editing (equal). **J. S. Armand Eyebe Fouda:** Conceptualization (equal); Data curation (equal); Formal analysis (equal); Investigation (equal); Methodology (equal); Project administration (equal); Supervision (equal); Validation (equal); Writing – original draft (equal); Writing – review & editing (equal). **Wolfram Koepf:** Formal analysis (equal); Methodology (equal); Validation (equal); Visualization (equal); Writing – original draft (equal); Writing – review & editing (equal).

DATA AVAILABILITY

No data were stored as the paper presents an online experiment. The pictures used in the paper are available from the corresponding author upon reasonable request.

REFERENCES

[1] C. Bandt and B. Pompe, "Permutation entropy: A natural complexity measure for time series," Phys. Rev. Lett. **88**, 174102 (2002).

[2] S. M. Bruijn, D. J. Bregman, O. G. Meijer, P. J. Beek, and J. H. van Dieën, "Maximum Lyapunov exponents as predictors of global gait stability: A modelling approach," Med. Eng. Phys. **34**, 428–436 (2012).

[3] G. A. Gottwald and I. Melbourne, "The 0-1 test for chaos: A review," in *Chaos Detection and Predictability* (Springer, 2016), pp. 221–247.

[4] J. S. A. Eyebe Fouda, B. Bodo, S. L. Sabat, and J. Y. Effa, "A modified 0-1 test for chaos detection in oversampled time series observations," Int. J. Bifurc. Chaos **24**, 1450063 (2014).

[5] A. Wolf, J. B. Swift, H. L. Swinney, and J. A. Vastano, "Determining Lyapunov exponents from a time series," Phys. D **16**, 285–317 (1985).

[6] Y. B. Pesin, "Characteristic Lyapunov exponents and smooth ergodic theory," Russ. Math. Surv. **32**, 55 (1977).

[7] V. Latora and M. Baranger, "Kolmogorov-Sinai entropy rate versus physical entropy," Phys. Rev. Lett. **82**, 520 (1999).

[8] C. Bogaert, F. Beckers, D. Ramaekers, and A. E. Aubert, "Analysis of heart rate variability with correlation dimension method in a normal population and in heart transplant patients," Auton. Neurosci. **90**, 142–147 (2001).

[9] E. Thelen and L. B. Smith, "Dynamic systems theories," in *Handbook of Child Psychology: Theoretical Models of Human Development*, edited by W. Damon and R. M. Lerner (John Wiley & Sons Inc., 1998), pp. 563–634.

[10] A. M. Unakafov and K. Keller, "Conditional entropy of ordinal patterns," Phys. D **269**, 94–102 (2014).

[11] D. Zhou, Q. Liu, J. C. Platt, C. Meek, and N. B. Shah, "Regularized minimax conditional entropy for crowdsourcing," arXiv:1503.07240 (2015).

[12] J. S. A. Eyebe Fouda and W. Koepf, "Detecting regular dynamics from time series using permutations slopes," Commun. Nonlinear Sci. Numer. Simul. **27**, 216–227 (2015).

[13] J. S. A. Eyebe Fouda, "Applicability of the permutation largest slope entropy to strange nonchaotic attractors," Nonlinear Dyn. **87**, 1859–1871 (2017).

[14] T. Haddad, N. Ben-Hamida, L. Talbi, A. Lakhssassi, and S. Aouini, "Temporal epilepsy seizures monitoring and prediction using cross-correlation and chaos theory," Healthc. Technol. Lett. **1**, 45–50 (2014).

[15] S. Tagne, B. Bodo, G. F. V. A. Eyebe, and J. S. A. Eyebe Fouda, "PIC microcontroller based synchronization of two fractional order jerk systems," Sci. Rep. **12**, 14281 (2022).

[16] E. E. García-Guerrero, E. Inzunza-González, O. R. López-Bonilla, J. R. Cárdenas-Valdez, and E. Tlelo-Cuautle, "Randomness improvement of chaotic maps for image encryption in a wireless communication scheme using PIC-microcontroller via ZigBee channels," Chaos, Solitons Fractals **133**, 109646 (2020).

[17] M. Small, D. Yu, I. Grubb, J. Simonotto, K. Fox, and R. Harrison, "Automatic identification and recording of cardiac arrhythmia," in *Computers in Cardiology 2000. Vol. 27 (Cat. 00CH37163)* (IEEE, 2000), pp. 355–358.

[18] J. S. A. Eyebe Fouda, "The matching energy: A novel approach for measuring complexity in time series," Nonlinear Dyn. **86**, 2049–2060 (2016).

[19] S. S. Parmar and A. P. Gharge, "R-2R ladder circuit design for 32-bit digital-to-analog converter (DAC) with noise analysis and performance parameters," in *2016 International Conference on Communication and Signal Processing (ICCSP)* (IEEE, 2016), pp. 0467–0471.

[20] S. Wiggins, "Chaos in the quasiperiodically forced Duffing oscillator," Phys. Lett. A **124**, 138–142 (1987).

[21] A. Sharma, V. Patidar, G. Purohit, and K. Sud, "Effects on the bifurcation and chaos in forced Duffing oscillator due to nonlinear damping," Commun. Nonlinear Sci. Numer. Simul. **17**, 2254–2269 (2012).

[22] G. Wang and S. He, "A quantitative study on detection and estimation of weak signals by using chaotic Duffing oscillators," IEEE Trans. Circuits Syst. I: Fundam. Theory Appl. **50**, 945–953 (2003).

[23] J. S. A. Eyebe Fouda, B. Bodo, G. M. Djeufa, and S. L. Sabat, "Experimental chaos detection in the Duffing oscillator," Commun. Nonlinear Sci. Numer. Simul. **33**, 259–269 (2016).

[24] B. Bodo, J. S. A. Fouda, E. Fouda, A. Mvogo, and S. Tagne, "Experimental hysteresis in memristor based Duffing oscillator," Chaos, Solitons Fractals **115**, 190–195 (2018).

[25] J. S. A. Eyebe Fouda, "Applicability of ordinal-array-based indicators to strange nonchaotic attractors," Ph.D. thesis, Universität Kassel, 2017.

10 April 2025 11:56:13